

Supersymmetry at LHC

S. ASAI

*International Centre for Elementary Particle Physics, University of Tokyo,
7-3-1 Bunkyo-ku, Hongo, Tokyo 113-0033, Japan
E-mail Shoji.Asai@cern.ch*

Abstract

This document describes prospects for discovering Supersymmetry and studying its properties at Large Hadron Collider(LHC). ATLAS and CMS collaborations have enormous potential to discover Supersymmetry, if it exists at mass scale less than about 2 TeV. Methods and potentials to determine the properties of SUSY particles using various kinematic distributions are also summarised.

This note contributes to proceedings of LHC symposium 2001

1 Introduction

Supersymmetric (SUSY) standard models [1] are most promising extensions of the standard model, because the SUSY can naturally deal with the problem of the quadratic Higgs mass divergence. In these theories, each elementary particle has a superpartner whose spin differs by $1/2$ from that of the particle. Discovery of these SUSY particles is one of important purpose of the ATLAS [2] and CMS [3] collaborations at LHC.

Although there are, in general, more than 100 free parameters to describe SUSY soft breaking [1], two predictable and promising SUSY models are summarised in this document.

- Super-Gravity Model [4] assumes that gravity is responsible for the mediation of the SUSY breaking and provides a natural candidate for cold dark matter [5]. Studies based on this model are summarised in Sec. 2. Precise measurements on masses of supersymmetric particles are described in Sec. 2.4. Discovery potential beyond minimal model is also shown in Sec. 3.
- Gauge-Mediated Model [6] assumes that standard model gauge interactions are responsible for the mediation. This model has a benefit to explain naturally why flavour changing neutral current is suppressed. Sec. 4 is devoted to studies on this model.

Studies in these sections are based on R-parity conservation [7], and violating case is mentioned in Sec. 5.

2 Minimal Super-Gravity Model

2.1 Introduction and production processes

Minimal Super-Gravity Model (mSUGRA) [4] is a special case of the Minimal Supersymmetric Model (MSSM). In this model, the SUSY soft breaking terms are assumed to be communicated from the SUSY breaking sector by

gravity. Furthermore, these SUSY soft breaking terms are universal at the GUT scale. There are only five parameters after imposing GUTs conditions;

- m_0 : Universal mass of all scalar particles at GUT scale.
- $m_{1/2}$: Universal mass of all gauginos at GUT scale.
- A_0 : Common trilinear coupling at GUT scale.
- $\tan\beta(\equiv v_2/v_1)$: Ratio of VEV of two Higgs fields at the Electroweak scale.
- $\text{sign}\mu$: ± 1 , Sign of Higgsino mass term.

Masses of gluino, \tilde{g} and gauginos are mainly determined by $m_{1/2}$. \tilde{g} becomes heavy due to large radiative corrections, and its mass is approximately $2.6 m_{1/2}$. Higgsino mass ($|\mu|$) becomes larger than gaugino mass at the EW scale, except for the case of $m_0 \gg m_{1/2}$. Then the lighter states of neutralino, $\tilde{\chi}_1^0$ and $\tilde{\chi}_2^0$, become almost pure gaugino states ($\tilde{\chi}_1^0 \sim \tilde{B}^0$, $\tilde{\chi}_2^0 \sim \tilde{W}^0$), and lighter state of chargino, $\tilde{\chi}_1^\pm$, is also gaugino-like ($\tilde{\chi}_1^\pm \sim \tilde{W}^\pm$). Scalar lepton masses are determined mainly by m_0 and weakly by $m_{1/2}$. On the other hand, scalar quark masses depend on both m_0 and $m_{1/2}$.

- $m(\tilde{g}) \sim 2.6 m_{1/2}$.
- $m(\tilde{\chi}_1^0) \sim 0.4 m_{1/2}$.
- $m(\tilde{\chi}_2^0) \sim m(\tilde{\chi}_1^\pm) \sim 0.8 m_{1/2}$.
- $m(\tilde{\ell}_R) \sim \sqrt{m_0^2 + 0.15m_{1/2}^2}$
- $m(\tilde{\ell}_L) \sim \sqrt{m_0^2 + 0.5m_{1/2}^2}$
- $m(\tilde{q}_{L,R}) \sim \sqrt{m_0^2 + 6m_{1/2}^2}$

Masses of 3rd generation scalar fermions (\tilde{t}_1 , \tilde{b}_1 , and $\tilde{\tau}_1$) depend also on A and $\tan\beta$ [8], and they are generally lighter than first and second generations because of the following two reasons. Firstly, one loop radiative

corrections to these masses are always negative, and corrections are proportional to Yukawa coupling. Secondly, the supersymmetric partners of the right-handed and left-handed states mix, and the resultant two mass eigenstates have a large mass splitting. This mixing contribution depends on both A_0 and $\tan\beta$.

Dominant SUSY production processes at LHC are $\tilde{g}\tilde{g}$, $\tilde{g}\tilde{q}$ and $\tilde{q}\tilde{q}$ through the strong interaction. These production cross-sections, σ , do not strongly depend on the SUSY parameters except for masses of \tilde{g} and \tilde{q} [9]. When these masses are 500 GeV, $\tilde{g}\tilde{g}$ is main production process, and total $\sigma(\tilde{g}\tilde{g}, \tilde{g}\tilde{q}$ and $\tilde{q}\tilde{q})$ is 100 pb. σ is 3 pb for $m_{\tilde{q}}=m_{\tilde{g}}=1\text{TeV}$. Even when these masses are 2 TeV, sizable σ of about 20 fb is expected. $\tilde{u}\tilde{u}$ and $\tilde{u}\tilde{d}$ are main production processes for such a heavy case, since u and d quarks are valence quarks. K-factors are about 1.4 [10] for the $\tilde{g}\tilde{g}$, $\tilde{g}\tilde{q}$ and $\tilde{q}\tilde{q}$ production processes (virtual effect), it is modest value as same as the case of Higgs boson. But all studies presented in this document are based on Leading Order Monte Carlo simulations [11, 12].

2.2 Decay processes

Decay modes of \tilde{g} and \tilde{q} are controlled by the mass-relation between each other, and are summarised in table 1. If kinematically possible, they decay into 2-body through the strong interaction. Otherwise, they decay into a electroweak gaugino plus quark(s). Bino/Wino-eigenstates presented in this table become simply mass-eigenstate, ($\tilde{B}^0 \sim \tilde{\chi}_1^0$, $\tilde{W}^0 \sim \tilde{\chi}_2^0$, and $\tilde{W}^\pm \sim \tilde{\chi}_1^\pm$), when m_0 is not too larger than $m_{1/2}$. In this case, Higgsino mass ($|\mu|$) becomes larger than gaugino mass at the EW scale, then Higgsino component decouples from lighter mass-eigenstates as already mentioned. Decay modes of third generation squarks (\tilde{t}_1 and \tilde{b}_1) are more complicated, since they have enough coupling to Higgsino due to non-negligible Yukawa couplings.

There are four leading decay modes of $\tilde{\chi}_2^0$ depending on mass spectrum. These are summarised in table 2 with the conditions of mass spectrum.

Table 1: Decay modes of \tilde{g} and \tilde{q} of 1st and 2nd generations. Branching fractions of $\tilde{g} \rightarrow t\tilde{t}$ and $\tilde{g} \rightarrow b\tilde{b}$

depend strongly on mass-relation between \tilde{g} and \tilde{t}/\tilde{b} .

	$m_{\tilde{q}} > m_{\tilde{g}}$	$m_{\tilde{q}} \sim m_{\tilde{g}}$	$m_{\tilde{q}} < m_{\tilde{g}}$
\tilde{g}	$\tilde{g} \rightarrow q\bar{q}\tilde{B}^0$ (~ 1) $q\bar{q}\tilde{W}^0$ (~ 2) $q\bar{q}\tilde{W}^\pm$ (~ 4)		$\tilde{g} \rightarrow q\tilde{q}$
	$\tilde{g} \rightarrow t\tilde{t}$ $b\tilde{b}$		
\tilde{q}_R	$\tilde{q}_R \rightarrow q\tilde{g}$	$\tilde{q}_R \rightarrow q\tilde{B}^0$	
\tilde{q}_L	$\tilde{q}_L \rightarrow q\tilde{g}$	$\tilde{q}_L \rightarrow q\tilde{W}^0$ (~ 1) $q\tilde{W}^\pm$ (~ 2)	

Table 2: Summary of decay modes of $\tilde{\chi}_2^0$

decay mode	condition and remarks
$\tilde{\chi}_2^0 \rightarrow \tilde{\ell}\ell$ $\rightarrow \ell\tilde{\chi}_1^0$	$m_{\tilde{\ell}} < m_{\tilde{\chi}_2^0}$ (Remarks) $\tilde{\chi}_2^0 \rightarrow \tilde{\tau}\tau$ for ($\tan\beta \gg 1$)
$\tilde{\chi}_2^0 \rightarrow h\tilde{\chi}_1^0$	$m_{\tilde{\chi}_2^0} - m_{\tilde{\chi}_1^0} > m_h$
$\tilde{\chi}_2^0 \rightarrow Z^0\tilde{\chi}_1^0$	$m_h > m_{\tilde{\chi}_2^0} - m_{\tilde{\chi}_1^0} > m_{Z^0}$
$\tilde{\chi}_2^0 \rightarrow f\bar{f}\tilde{\chi}_1^0$	3-body decay, other cases

When the scalar lepton, $\tilde{\ell}$, is lighter than $\tilde{\chi}_2^0$, 2-body decay chain, $\tilde{\chi}_2^0 \rightarrow \tilde{\ell}\ell(\rightarrow \ell\tilde{\chi}_1^0)$ becomes dominant decay mode. Branching fraction of $\tilde{\chi}_2^0 \rightarrow \tau\tilde{\tau}_1$ is significant large in the case of $\tan\beta \gg 1$. $\tilde{\chi}_2^0 \rightarrow h\tilde{\chi}_1^0$ is dominant mode, if the mass difference between $\tilde{\chi}_2^0$ and $\tilde{\chi}_1^0$ is larger than Higgs boson mass. When the mass difference is smaller than m_{Z^0} , three body decay is main decay process. $\tilde{\chi}_1^\pm$ has three leading decay modes, $\tilde{\chi}_1^\pm \rightarrow \tilde{\ell}\nu$, $W^\pm\tilde{\chi}_1^0$ and $f\bar{f}'\tilde{\chi}_1^0$ as the similar manner to $\tilde{\chi}_2^0$.

2.3 Event topologies of mSUGRA events and discovery potential

\tilde{g} and/or \tilde{q} are copiously produced at the LHC with $p_T \sim M$. High p_T jets are emitted from the decays of \tilde{g} and \tilde{q} as shown in table 1. Each event contains two $\tilde{\chi}_1^0$'s in the final state. If R-parity [7] is conserved, $\tilde{\chi}_1^0$ is stable, and it is neutral and weakly interacting and escape from the detection. Then missing transverse energy, \cancel{E}_T , carried away by two $\tilde{\chi}_1^0$'s plus multiple high p_T jets is the leading experimental signature of SUSY. Also the other activities of additional jets, leptons and $b\bar{b}$ are possible, coming from the decays of $\tilde{\chi}_2^0$ and $\tilde{\chi}_1^\pm$. These additional informations are important to confirm SUSY signals, and to investigate its properties.

The following four standard model processes can potentially have \cancel{E}_T event topology with jets.

- $W^\pm + \text{jets}, W^\pm \rightarrow \ell\nu$
- $Z^0 + \text{jets}, Z^0 \rightarrow \nu\bar{\nu}, \tau^+\tau^-$
- $t\bar{t}$
- QCD jets with mismeasurement

SUSY signals should be observed as an excess of these standard model processes. Large significance can be obtained for SUSY signals after large \cancel{E}_T and p_T are respectively required on event and jets. $\cancel{E}_T + \sum_{jets} p_T$ is a good variable [14] to see an excess coming from the SUSY signals as shown in Fig. 1. The distribution of $\cancel{E}_T + \sum_{jets} p_T$ has steep slop for the standard model background processes as shown in this figure. On the other hand, the distribution for the SUSY signals has a peak at large value, and long tail contribute to the higher side. The shape quite differs from that of the background processes. This peak position has a good sensitivity to $\min(m(\tilde{g}), m(\tilde{q}))$, and it can be determined with accuracy of 15% [13] using this variable. It will be discussed later. Independent excesses are also ex-

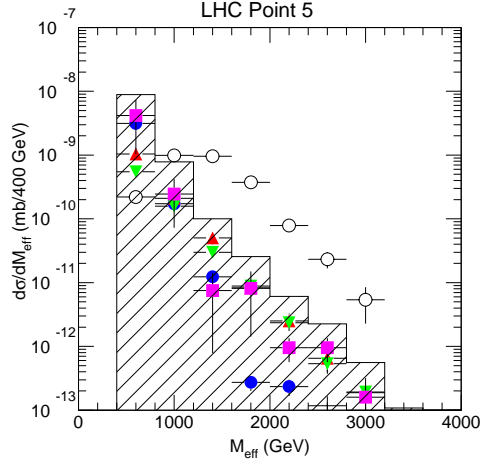


Figure 1: $\cancel{E}_T + \sum_{jets} p_T$ distributions: (open circles) for SUSY signals at LHC point 5 [14], and (histogram) for sum of all standard model backgrounds. It includes the followings: $t\bar{t}$ (black circles), $W^\pm + jets$ (triangles), $Z^0 + jets$ (downward-triangles), and QCD(squares).

pected in the other topologies, for example, $\cancel{E}_T + jets + isolated\ lepton(s)$. This isolated lepton will be emitted from $\tilde{\chi}_2^0$ and $\tilde{\chi}_1^\pm$.

Figure 2 shows 5σ -discovery potential in m_0 - $m_{1/2}$ plane for $\tan\beta = 35$ using the \cancel{E}_T plus jets channel with various integrated luminosities. Mass contours for \tilde{g} and \tilde{q} are also superimposed. As shown in this figure, \tilde{g} and \tilde{q} can be discovered close to $M \sim 1.5$ TeV with a luminosity of 1 fb^{-1} , which is corresponding to just one month run with $10^{33}\text{ cm}^{-2}\text{ s}^{-1}$. The interesting region for relic density of the dark matter is almost covered with just 1 fb^{-1} . \tilde{g} and \tilde{q} , whose masses are about 2.5 TeV, can be discovered finally with a luminosity of 300 fb^{-1} . This luminosity is corresponding to three years run with design luminosity of $10^{34}\text{ cm}^{-2}\text{ s}^{-1}$. Both ATLAS [14] and CMS [15] collaborations have an excellent potential to discover SUSY, and they will cover interesting parameter region predicted by naturalness [1] and relic density of dark matter [1, 5].

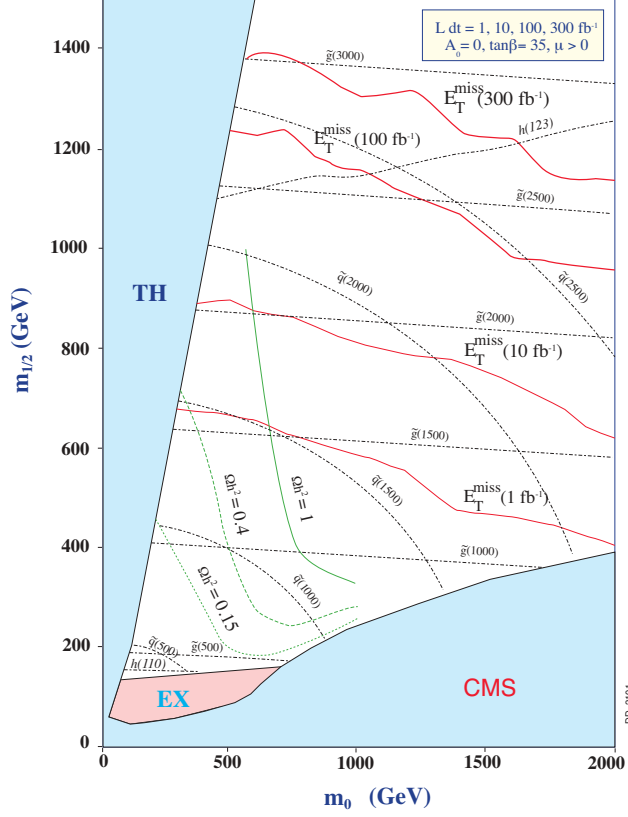


Figure 2: 5σ -discovery region in m_0 - $m_{1/2}$ plane for $\tan\beta = 35$ using the E_T plus jets channel. Mass contours for \tilde{g} and \tilde{q} are also superimposed. Ωh^2 shows relic density of the dark matters. In the gray region, $\tilde{\ell}$ becomes the LSP, or no electroweak symmetry breaking occurs.

2.4 Measurements of masses of SUSY particles

Since two undetected LSP's exist in each event, there are six unknown momentum components in addition to the $\tilde{\chi}_1^0$ mass. So no mass peak is expected in general. However it is possible to use kinematic end points of various distributions as follows [14, 15].

- (1) Select specific decay chain exclusively. For example,

$$\begin{aligned} \tilde{g} &\rightarrow \tilde{q}_L q \\ &\quad \rightarrow \tilde{\chi}_2^0 q \\ &\quad \quad \rightarrow \tilde{\ell} \ell \\ &\quad \quad \quad \rightarrow \tilde{\chi}_1^0 \ell \end{aligned}$$

- (2) Make various distributions of invariant masses and p_T .
- (3) kinematic constraints are obtained from edges and end points of these distributions. These edges and end points are combinations of the masses, and these are just determined by the kinematics and not depend on the other SUSY parameters.

If there are at least three 2-body decays like this example, full reconstruction of masses is possible model-independently. It is important remark. When we can not find out such three 2-body decays, number of obtained constraint is less than number of unknown masses. Some assumption is necessary to determine mass spectrum of SUSY. SUSY events become background itself for detailed study, since there are many cascade decay patterns in \tilde{q} and \tilde{g} .

2.4.1 Kinematic edges for $\tilde{\chi}_2^0$ decay:

$\tilde{\chi}_2^0 \rightarrow \ell \tilde{\ell} (\rightarrow \ell + \tilde{\chi}_1^0)$ is the dominant decay mode, when $\tilde{\ell}$ is lighter than $\tilde{\chi}_2^0$. This is corresponding to the parameter space of $m_0 < \sim 0.8m_{1/2}$.

The same flavour opposite charge di-lepton ($\ell = e, \mu$) is the characteristic signal. Left side of Fig. 3 shows invariant mass distribution of the

di-lepton system. Flavour subtraction, $e^+e^- + \mu^+\mu^- - e^+\mu^- - e^-\mu^+$, has been performed to suppress flat distribution comes from chargino and $t\bar{t}$ decays. Sharp edge ($M_{\ell\ell}^{max}$) is observed, and it is related to

$$M_{\ell\ell}^{max} = m(\tilde{\chi}_2^0) \sqrt{1 - (m(\tilde{\ell})/m(\tilde{\chi}_2^0))^2} \sqrt{1 - (m(\tilde{\chi}_1^0)/m(\tilde{\ell}))^2}. \quad (1)$$

This can be determined very precisely. Statistical error is 0.1% with $L=100 \text{ fb}^{-1}$ for this case (it strongly depends on $\sigma \times \text{Br}$), and systematic error is less than 0.1%, mainly comes from uncertainty of the energy scale calibration. Figure 4 shows the parameter region in which $M_{\ell\ell}^{max}$ can be determined. $M_{\ell\ell}^{max}$ originated from 2-body decay ($\tilde{\chi}_2^0 \rightarrow \tilde{\ell}_L \ell$ and $\tilde{\chi}_2^0 \rightarrow \tilde{\ell}_R \ell$) can be observed in a wide region as presented in this figure.

Furthermore, an asymmetry of p_T of two leptons,

$$A_{\ell\ell} = \frac{p_T^{max} - p_T^{min}}{p_T^{max} + p_T^{min}}, \quad (2)$$

has also information on $\tilde{\ell}$ mass [16]. As $\tilde{\ell}$ mass is heavier, asymmetry, $A_{\ell\ell}$, becomes larger. Above two kinematic constraints are obtained from the di-lepton system.

When $\tan \beta$ is much larger than 1, $\tilde{\tau}_1$ becomes much lighter than \tilde{e}_R and $\tilde{\mu}_R$, and $\tilde{\chi}_2^0 \rightarrow \tilde{\tau}_1 \tau$ can become dominant decay mode [17]. Hadronic decay mode of τ is used for a τ -identification. The followings are essence of the τ -identification, and the selection efficiency is about 40%:

- 1-3 prong is selected.
- Energy deposited in calorimeter and these tracks are well concentrated in narrow cone($R=0.2$).
- This activity are well isolated from jet activities.

Right side of Fig. 3 shows $M_{\tau\tau}$ distribution, which is visible invariant mass of $\tau\tau$ system times $1/0.66$. This factor is mean value to correct the energy carried by neutrinos. Flat contribution in this distribution comes

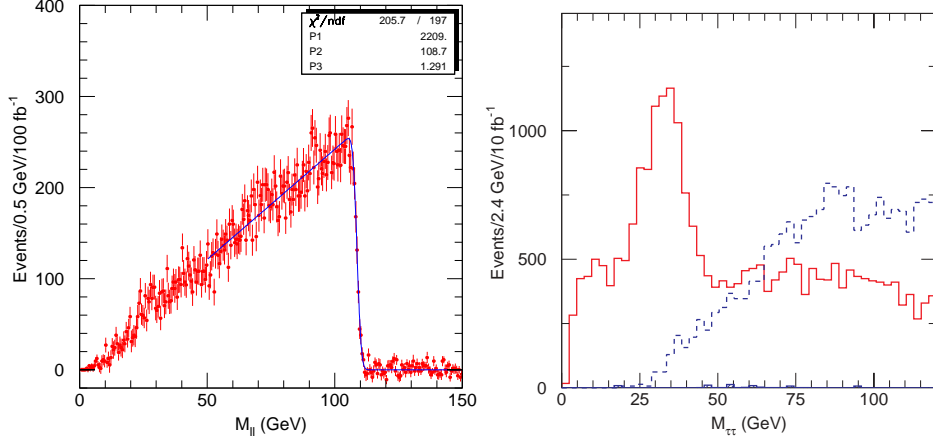


Figure 3: (Left) Invariant mass distribution for the di-lepton system (e^+e^- and $\mu^+\mu^-$) (at LHC point 5 [14]). Flavour subtraction, $e^+e^- + \mu^+\mu^- - e^+\mu^- - e^-\mu^+$, has been performed. (Right) Invariant mass distribution for identified τ -pair system (at LHC point 6). Solid line shows distribution for the correct τ -pair, and dotted line shows the contribution from fake τ .

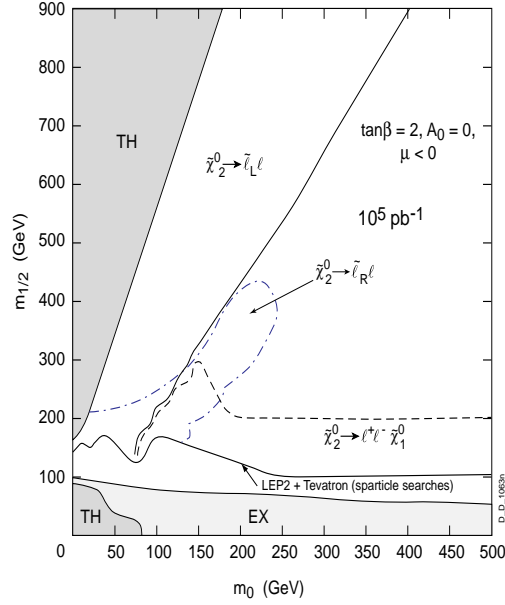


Figure 4: Parameter region for observing the edge of $M_{\ell+\ell^-}$ due to $\tilde{\chi}_2^0 \rightarrow \tilde{l}_L \ell$ (solid), $\tilde{\chi}_2^0 \rightarrow \tilde{l}_R \ell$ (dashed-dotted) and $\tilde{\chi}_2^0 \rightarrow \ell^+ \ell^- \tilde{\chi}_1^0$ (dashed).

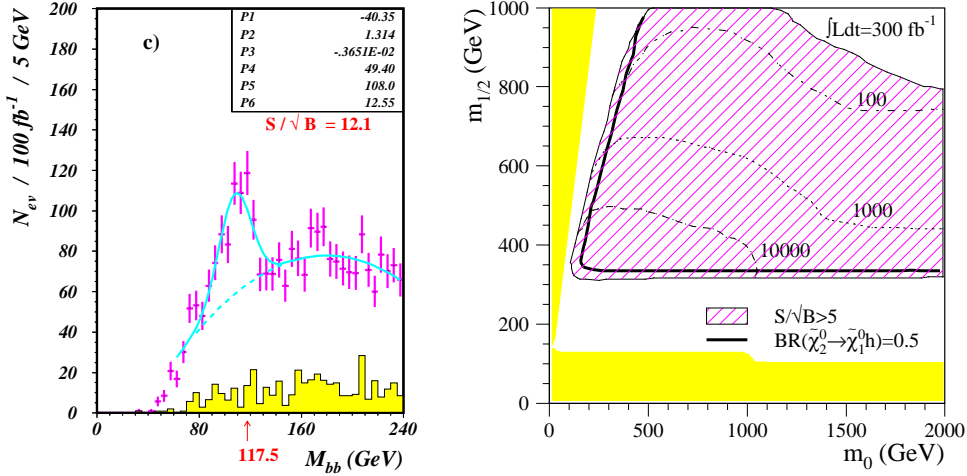


Figure 5: (Left) Invariant mass distribution for $b\bar{b}$ system for $\tan\beta=10$ ($m_0=m_{1/2}=500$ GeV and $\mu < 0$). Hatched histogram shows the background contribution from the standard model processes. (Right) 5σ -visibility contour in m_0 - $m_{1/2}$ plane for $\tan\beta=10$ with luminosity of 300 fb^{-1} .

from $\tilde{\chi}_1^\pm \rightarrow \tilde{\tau}\nu$. Kinematic edge can be also observed even in the τ case, and this can be determined with accuracy of about 5%. This edge is related to various masses in eq.(1).

$\tilde{\chi}_2^0 \rightarrow h\tilde{\chi}_1^0$ becomes the dominant decay mode, when $\tilde{\ell}$ is heavier than $\tilde{\chi}_2^0$ and the mass difference between $\tilde{\chi}_2^0$ and $\tilde{\chi}_1^0$ is larger than m_h . It is corresponding to the parameter space of $0.4 m_{1/2} > m_h$. Fig. 5(Left) shows the $M_{b\bar{b}}$ distribution, and a clear peak is observed at Higgs boson mass. This peak can be seen with more than 5σ -significance in a wide parameter region as shown in right side of Fig. 5. Events in this peak can be used for reconstruction of decay chain including $\tilde{\chi}_2^0$ as mentioned later. Events with $\tilde{\chi}_2^0 \rightarrow Z^0\tilde{\chi}_1^0$ also can be used in the same manner.

Figures 6 show invariant mass distributions of same flavour opposite charge di-lepton ($\ell = e, \mu$) system for the 3-body decay of $\tilde{\chi}_2^0$. This decay mode becomes dominant, when the mass difference between $\tilde{\chi}_2^0$ and $\tilde{\chi}_1^0$ is smaller than M_Z . Sharp kinematic edges ($M_{\ell\ell}^{max}$) are observed in both parameter points. Figure 4 shows the parameter region in which the $M_{\ell\ell}^{max}$

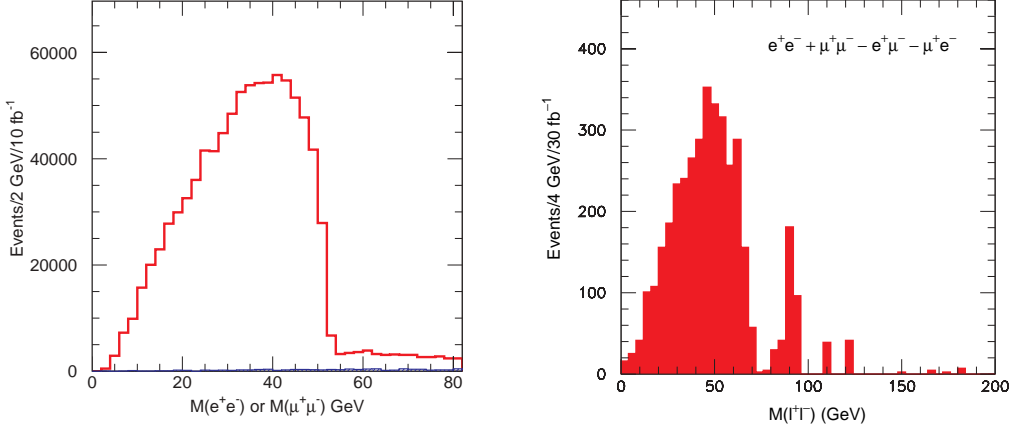


Figure 6: Invariant mass distributions for di-lepton system (e^+e^- and $\mu^+\mu^-$) Left histogram shows the case of small m_0 (at LHC point 3) and right shows large m_0 (at LHC point 4).

can be determined with $L=100 \text{ fb}^{-1}$. $M_{\ell\ell}^{max}$ originated from 3-body decay can be observed in wide region. $M_{\ell\ell}^{max}$ is related to mass difference between $\tilde{\chi}_2^0$ and $\tilde{\chi}_1^0$, i.e.

$$M_{\ell\ell}^{max} = m(\tilde{\chi}_2^0) - m(\tilde{\chi}_1^0). \quad (3)$$

This kinematic edge can be determined very precisely as the same as 2-body decay case.

For $\ell^+\ell^-$ near the kinematic end point, momentum of $\tilde{\chi}_2^0$ in Lab-frame, $\vec{P}(\tilde{\chi}_2^0)$, can be directly reconstructed event by event, since $\ell^+\ell^-$ and $\tilde{\chi}_1^0$ almost stand still in $\tilde{\chi}_2^0$ rest-frame.

$$\vec{P}(\tilde{\chi}_2^0) = (1 + m(\tilde{\chi}_1^0)/m(\ell^+\ell^-))\vec{P}(\ell\ell) \quad (4)$$

Four-momentum of $\tilde{\chi}_2^0$ can be reconstructed assuming relation between $m(\tilde{\chi}_1^0)$ and $m(\tilde{\chi}_2^0)$, since mass difference between $\tilde{\chi}_1^0$ and $\tilde{\chi}_2^0$ is already measured from the kinematic edge.

Sharp peak is also observed at M_Z in right side of Fig. 6. This is contribution from the heavier state of chargino ($\tilde{\chi}_2^\pm$) and neutralino ($\tilde{\chi}_4^0$). When m_0 is much larger than $m_{1/2}$, Higgsino mass ($|\mu|$) is relatively small comparing

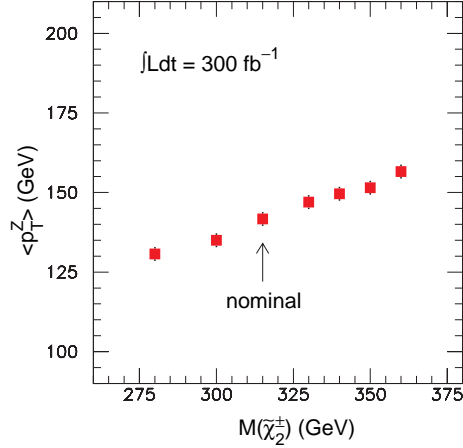


Figure 7: Mean value of p_T^Z as function of $\tilde{\chi}_2^\pm$ -mass.

Wino mass (otherwise, electroweak symmetry breaking has problem), then the resultant mass eigenstates of chargino and neutralino become the mixed states of Higgsinos and Wino. In such a case, there is substantial branching fraction of $\tilde{g} \rightarrow \tilde{\chi}_2^\pm f \bar{f}$, and Z^0 are produced from $\tilde{\chi}_2^\pm$. Momentum of the reconstructed Z^0 carries an information about mass of the parent chargino, $\tilde{\chi}_2^\pm$, as shown in Fig. 7. Since a mean value of p_T^Z , $\langle p_T^Z \rangle$, is proportional to the $\tilde{\chi}_2^\pm$ mass, it can be determined by the fitted $\langle p_T^Z \rangle$ with an accuracy of 3% including systematic errors.

2.4.2 Kinematic end points of jets plus $\tilde{\chi}_2^0$:

$\tilde{\chi}_2^0$ is emitted mainly from $\tilde{q}_L \rightarrow q \tilde{\chi}_2^0$ and $\tilde{g} \rightarrow q \bar{q} \tilde{\chi}_2^0$ processes as presented in table 1. An information about mass of the parent particles, \tilde{q}_L and \tilde{g} , can be obtained as follows.

$$\begin{aligned}
\tilde{q}_L &\rightarrow \tilde{\chi}_2^0 q \\
&\rightarrow \tilde{\ell} \ell \\
&\quad \rightarrow \tilde{\chi}_1^0 \ell \quad (2\text{-body decay chain}) \\
&\rightarrow \ell \ell \tilde{\chi}_1^0 \quad (3\text{-body decay}) \\
&\rightarrow h \tilde{\chi}_1^0 \\
&\quad \rightarrow b \bar{b} \quad (h \text{ decay})
\end{aligned}$$

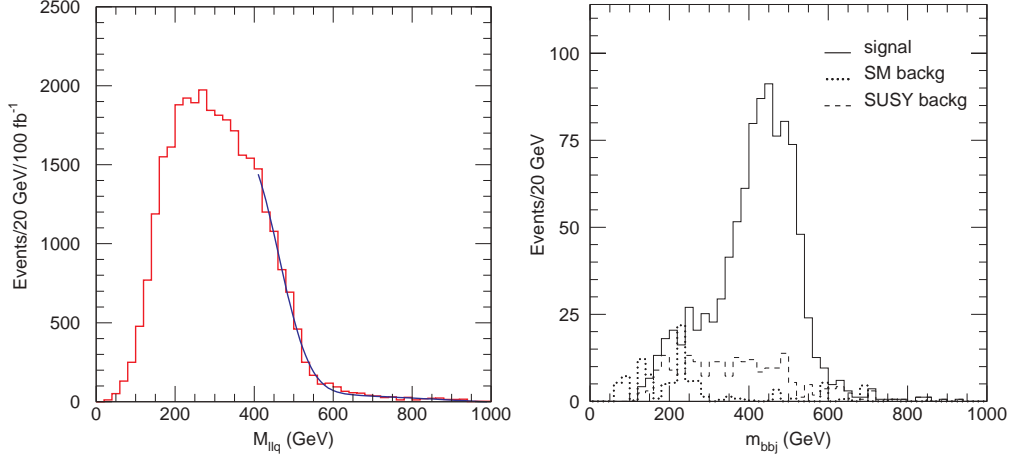


Figure 8: (Left) Invariant mass distributions of $q\ell\ell$ (at LHC point 5). (Right) Invariant mass distributions of qbb (at LHC point 1).

are the leading decay chains of \tilde{q}_L . Figures 8 show invariant mass distributions of $q\ell\ell$ - and qbb -systems. Although distributions are smeared by the limited energy resolution for hadron jets, these distributions have kinematic end points. Effects of the energy resolution and gluon emission from q should be taken into account to determine the end point. These kinematic end points are related to

$$\begin{aligned}
 M_{\ell\ell q}^{max} &= \frac{\sqrt{m(\tilde{q}_L)^2 - m(\tilde{\chi}_2^0)^2} \sqrt{m(\tilde{\chi}_2^0)^2 - m(\tilde{\chi}_1^0)^2}}{m(\tilde{\chi}_2^0)} \\
 (M_{h\tilde{q}}^{max})^2 &= m(h)^2 + \frac{m(\tilde{q}_L)^2 - m(\tilde{\chi}_2^0)^2}{2m(\tilde{\chi}_2^0)^2} \\
 &\times \left(m(\tilde{\chi}_2^0)^2 + m(h)^2 - m(\tilde{\chi}_1^0)^2 + \sqrt{(m(\tilde{\chi}_2^0)^2 - m(h)^2 - m(\tilde{\chi}_1^0)^2)^2 - 4m(h)^2 m(\tilde{\chi}_1^0)^2} \right)
 \end{aligned} \tag{5}$$

and can be determined with an accuracy of a few %.

For 3-body decay of $\tilde{\chi}_2^0$, four-momentum of $\tilde{\chi}_2^0$ can be directly reconstructed assuming the relation between $m(\tilde{\chi}_1^0)$ and $m(\tilde{\chi}_2^0)$ as already mentioned. An Invariant mass distribution of jet and reconstructed $\tilde{\chi}_2^0$ is shown

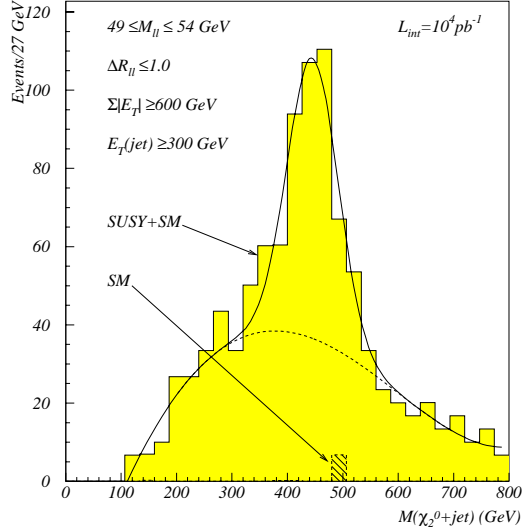


Figure 9: Invariant mass distribution of jet and the reconstructed $\tilde{\chi}_2^0$ for $m_0=300$ GeV, $m_{1/2}=150$ GeV and $\tan\beta=2$. Dotted line shows combinatorial background.

in Fig. 9. A peak appears at $m(\tilde{q}_L)$ and this can be determined directly with an accuracy of 5% including systematic errors.

There are four unknown masses (\tilde{q}_L , $\tilde{\chi}_2^0$, $\tilde{\ell}$ and $\tilde{\chi}_1^0$) in the following 2-body decay chain:

$$\begin{aligned}
 \tilde{q}_L &\rightarrow \tilde{\chi}_2^0 q \\
 &\rightarrow \tilde{\ell} \ell \\
 &\rightarrow \tilde{\chi}_1^0 \ell,
 \end{aligned}$$

which is dominant mode in the parameter space of $m_0 < 0.8m_{1/2}$. Figure 3(left), 8(left) and 10 show the invariant mass distributions of $\ell\ell$, $\ell\ell+\text{jet}$, and $\ell+\text{jet}$. Three kinematic end points and one threshold of 4-body system ($\ell^+\ell^-\tilde{q}\tilde{\chi}_1^0$) are observed in these figures, and **all four unknown masses can be determined model-independently**. Although errors of these determined masses are strongly correlated, accuracies of these masses are 3, 6, 9 and 12% for $m(\tilde{q}_L)$, $m(\tilde{\chi}_2^0)$, $m(\tilde{\ell})$ and $m(\tilde{\chi}_1^0)$, respectively. We can examine

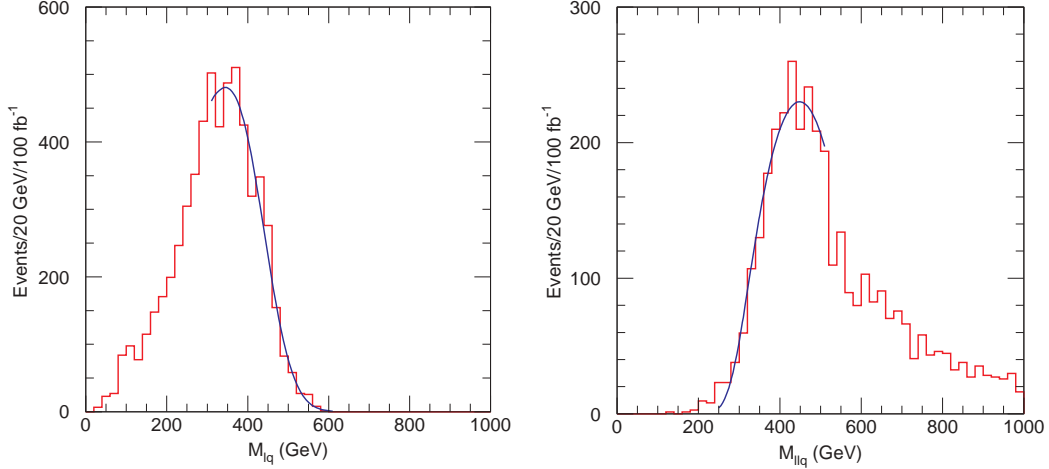


Figure 10: Invariant mass distributions of $q\ell$ and $q\ell\ell$ (at LHC point 5).

SUSY model using the model-independent measurement [18]. Furthermore, there is one more constraint from $A_{\ell\ell}$ defined in eq.(2). Thus four unknown masses can be fitted with five constraints(1C fit) for this 2-body decay chain.

Following decay chains of \tilde{g} is used to obtain an information about \tilde{g} mass.

$$\begin{aligned}
 \tilde{g} &\rightarrow \tilde{\chi}_2^0 q\bar{q} \\
 &\quad \rightarrow \ell\ell\tilde{\chi}_1^0 \\
 &\rightarrow \tilde{\chi}_1^\pm q\bar{q} \\
 &\quad \rightarrow \ell\nu\tilde{\chi}_1^0
 \end{aligned}$$

Four high p_T jets and three leptons are required to select $\tilde{g}\tilde{g}$ events. Figure 11 shows the invariant mass distribution of two high p_T jets. Since $\tilde{\chi}_2^0$ and $\tilde{\chi}_1^\pm$ are almost always nearly degenerate [1], the end point of M_{jj} is observed at the mass difference between \tilde{g} and $\tilde{\chi}_2^0/\tilde{\chi}_1^\pm$. This can be determined with an accuracy of 1.5%. Main systematic error comes from uncertainty of calibration of jet energy scale (1%). Three masses of \tilde{g} , $\tilde{\chi}_2^0(\tilde{\chi}_1^\pm)$ and $\tilde{\chi}_1^0$ can be determined assuming the relation between $m(\tilde{\chi}_1^0)$ and $m(\tilde{\chi}_2^0)$.

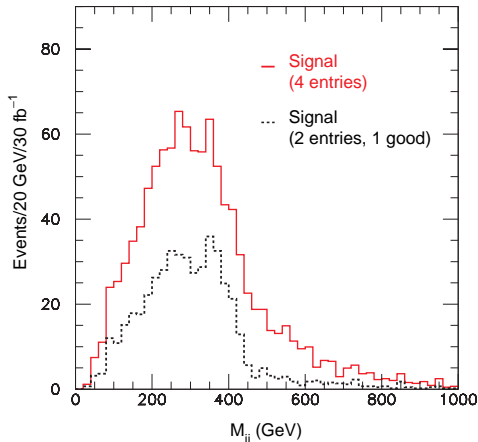


Figure 11: Invariant mass distributions of two jets (at LHC point 4). Solid line shows all combinations. Combinations of two hardest jets and two softest jets are rejected to obtain correct combinations (dotted line).

Dominant decay mode of \tilde{q}_R is $\tilde{q}_R \rightarrow q\tilde{\chi}_1^0$. Kinematic end point of p_T distribution of the highest p_T -jet is related to $m(\tilde{q}_R)$, since p_T^{max} is proportional to $\frac{1}{2}m(\tilde{q}_R)(1 - (m(\tilde{\chi}_1^0)/m(\tilde{q}_R))^2)$ in \tilde{q}_R rest-frame, and since $(m(\tilde{\chi}_1^0)/m(\tilde{q}_R))^2$ is expected to be small. $m(\tilde{q}_R)$ can be determined with an accuracy of a few %.

$\text{Min}(m(\tilde{q}), m(\tilde{g}))$ can be also determined by inclusive study. $\cancel{E}_T + \sum_{jets} p_T$ is proportional to $\text{min}(m(\tilde{q}_R), m(\tilde{g}))$ as shown in Fig. 12. It can be determined independently from the exclusive studies mentioned above. Accuracy is about 15% [13] including systematic errors, and large contributions come from the uncertainty of $\cancel{E}_T + \sum_{jets} p_T$ -distribution for the background processes.

2.5 Summary and comments on mSUGRA

$\tilde{\chi}_2^0$ plays an important role to determine masses of the SUSY particles, and studies have been done systematically [14, 15] for various decay modes presented in table 2. $\tilde{g} \rightarrow q\bar{q}\tilde{\chi}_2^0(\tilde{\chi}_1^\pm)$ and $\tilde{q} \rightarrow q\tilde{\chi}_{1,2}^0$ processes are useful to determine \tilde{g} or \tilde{q} mass as presented in Sec.2.4. Although all of \tilde{g} -, $\tilde{q}_{L/R}$ -, $\tilde{\ell}$ -, $\tilde{\chi}_2^0$ - and $\tilde{\chi}_1^0$ -mass can not be determined independently, many parts of

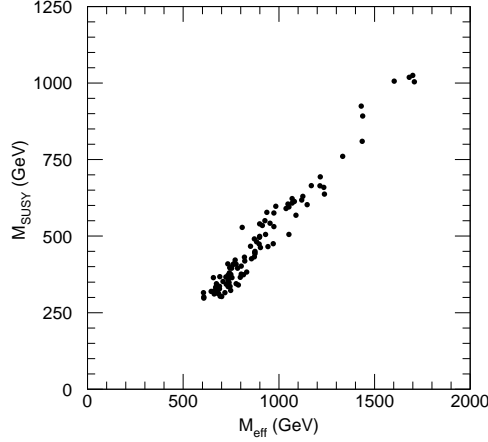


Figure 12: X-axis is fitted value of the peak of $E_T + \sum_{jets} p_T$ distribution. Y-axis is $\min(m(\tilde{q}_R), m(\tilde{g}))$. This relation is obtained in mSUGRA model.

Table 3: Determination of mSUGRA parameters ($L=30 \text{ fb}^{-1}$): ‘D’ and ‘ND’ mean ‘determined’ and ‘not determined’, respectively.

LHC point	m_0 (GeV)	$m_{1/2}$ (GeV)	A_0 (GeV)	$\tan \beta$	$\text{sign}(\mu)$
1	400 ± 100	400 ± 10	ND	2.0 ± 0.08	D
2	400 ± 100	400 ± 10	ND	10.0 ± 2.0	D
3	200 ± 10	100 ± 1	ND	2.0 ± 0.05	D
4	800 ± 50	200 ± 4	ND	10.0 ± 2.0	D with $L=300 \text{ fb}^{-1}$
5	$100^{+4.1}_{-2.2}$	300 ± 2.7	ND	2.0 ± 0.1	D
6	236 ± 37	200 ± 14	ND	41 ± 3.9	ND

the mSUGRA parameters can be determined [14] by global fit using these measurements on these end points, since there are strong correlations between these masses in the mSUGRA model. Fitted values of the mSUGRA parameters are summarised in table 3 for various LHC points. As mentioned in Sec.2.1, $m_{1/2}$ is determined mainly by $m(\tilde{\chi}_2^0)$ and $m(\tilde{g})$, and its error is smaller than 10%. $m(\tilde{q}_L)$ and $m(\tilde{\ell}_R)$ contribute to strong constraint on m_0 , whose accuracy is 5-20%. $\tan \beta$ is determined by Higgs boson mass.

When $|\mu|$ mass is not larger than wino mass ($\sim 0.8m_{1/2}$), the heavier states of chargino and neutralino also appear in the cascade decay chain of

\tilde{q} and \tilde{g} . Substantial branching fraction including $\tilde{\chi}_2^\pm$ and $\tilde{\chi}_4^0$;

$$\begin{aligned}\tilde{q} &\rightarrow \tilde{\chi}_2^\pm/\tilde{\chi}_4^0 + q \\ &\rightarrow \tilde{\chi}_2^0/\tilde{\chi}_1^\pm + Z^0/W^\pm \\ &\rightarrow \tilde{\chi}_1^0 + f\bar{f}\end{aligned}$$

is expected in this case. Event topology of such a decay chain is more complicated, but it is a good chance to measure $|\mu|$ directly. $|\mu|$ is important, since Higgsino plays important role to Electroweak symmetry breaking in Supersymmetry. It is necessary to study systematically decay chains involving $\tilde{\chi}_2^\pm$ and $\tilde{\chi}_4^0$.

Situations of 3rd generation \tilde{q} (\tilde{t} and \tilde{b}) are complicated but very important because of the following two reasons:

- These masses depend not only on m_0 and $m_{1/2}$ but also on A_0 , $\tan\beta$, and μ . Mass spectrum change drastically, then there are many decay pattern of \tilde{t} and \tilde{b} to be considered. Systematic study on the decay patterns is necessary, and the observed decay patterns will help us to understand A_0 , $\tan\beta$, and μ .
- \tilde{t} and \tilde{b} have large coupling to Higgsino, since Y_t and $Y_b(\tan\beta \gg 1)$ is very large. Then $\tilde{\chi}_2^\pm$ and $\tilde{\chi}_{3,4}^0$ appear in the decay chains, if kinematically possible. Event topology is more complicated than that of 1st and 2nd generations, but it is good chance to study Higgsino at LHC. It may have key of Electroweak symmetry breaking in Supersymmetry.

3 Beyond Minimal Super-Gravity Model

Phenomenological 9 parameters [1] are introduced to study SUSY signals beyond the **Minimal** SUGRA model. Parameters and used values are summarised in table 4. The GUT relations on gaugino masses (M_1, M_2 , and M_3) are relaxed, and universality of scalar sector are also relaxed. Totally 140k parameter sets are possible for these combinations. Current experimental

Table 4: Parameters in CMSSM model

Bino mass (M_1)	100, 500, 1000, 2000 GeV
Wino mass (M_2)	100, 500, 1000, 2000 GeV
\tilde{g} mass (M_3)	600–3000 GeV (300GeV step)
Higgsino mass (μ)	200, 500, 2000 GeV
$\tilde{\ell}$ mass	200, 1000, 3000 GeV
\tilde{q} mass	600–3000 GeV (300GeV step)
$\tan \beta$	2,50 GeV
M_A	200, 1000, 3000 GeV
A_0	0,2000 GeV

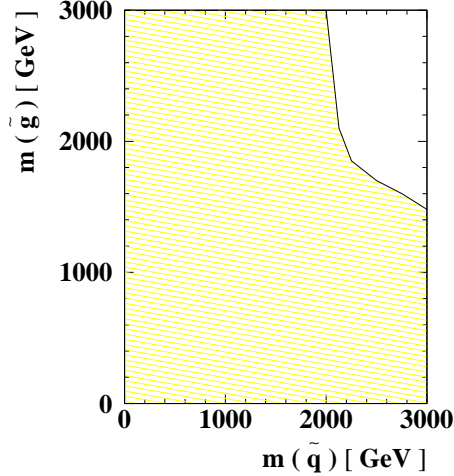


Figure 13: the 5- σ discovery potential in \tilde{g} - \tilde{q} mass plane with $L=100 \text{ fb}^{-1}$.

limits and theoretical constraints are applied to reduce the number of parameter sets. 20k parameter sets pass through these conditions, and these are examined.

Selections are optimised point by point on multi-dimensional space of $(\cancel{E}_T, N_{\text{lepton}}, p_T \text{ of lepton}, N_{\text{jets}}, p_T \text{ of jet}, \text{ and } \sum E_t)$. Figure 13 shows the 5- σ discovery potential in \tilde{g} - \tilde{q} mass plane. Even in this case, SUSY signals can be discovered up to 1.5 TeV (for \tilde{g}) and 2 TeV (for \tilde{q}), if mass difference between \tilde{g}/\tilde{q} and $\tilde{\chi}_1^0$ (LSP) is larger than about 200 GeV. This condition is not examined in this study, but it is necessary to ensure trigger.

4 Gauge Mediated SUSY Model

4.1 Introduction

Gauge Mediated SUSY breaking model (GMSB) [6] is alternative, but also attractive breaking scenario. In this model, SUSY breaking is assumed to be communicated by standard model gauge interactions. It can be explained very naturally why flavour changing neutral current is suppressed in this model.

- There are six parameters [6]; \sqrt{F} (SUSY breaking scale), M_m (mass scale of messenger sector), N_5 (Number of representation of messenger sector), C_{gra} (the ratio of the gravitino mass to the value in the case of if there is only SUSY breaking at \sqrt{F}), sign of μ and $\tan\beta$.
- Mass spectrum of SUSY particles is similar to mSUGRA, but the LSP is gravitino, \tilde{G} , whose mass is expected to be smaller than a few keV. \tilde{G} can be treated as massless particle at LHC. The next lightest supersymmetric particle (NLSP) is $\tilde{\ell}$ or $\tilde{\chi}_1^0$, it is important branch of event topology. Lifetime of NLSP is controlled by C_{gra} and \sqrt{F} , and it is also important branch of event topology. Event topologies are summarised in table 5.
- Dominant production processes at LHC are $\tilde{g}\tilde{g}$, $\tilde{g}\tilde{q}$ and $\tilde{q}\tilde{q}$ through strong interaction as the same as in SUGRA.
- Photons/leptons and E_T carried by \tilde{G} 's are the experimental signature. When NLSP is $\tilde{\ell}$ whose lifetime is longer, heavy charged stable particle becomes the experimental signature.

Event topologies with photons and heavy charged particle are are summarised in Sec.4.2 and 4.3.

4.2 Events with photons : $\tilde{\chi}_1^0 \rightarrow \tilde{G}\gamma$

This 2-body decay chain;

Table 5: Event topologies of GMSB signals

NLSP	Lifetime of NLSP	Event topology
$\tilde{\chi}_1^0$	Long ($c\tau > O(1)\text{m}$)	Same as mSUGRA
	Short	mSUGRA + photons $\tilde{\chi}_1^0 \rightarrow \tilde{G}\gamma$
$\tilde{\ell}$	Long	Heavy charged stable particles (Exotic)
	Short	mSUGRA + leptons

$$\begin{aligned}
 \tilde{\chi}_2^0 &\rightarrow \ell \tilde{\ell}_R \\
 &\rightarrow \ell \tilde{\chi}_1^0 \\
 &\rightarrow \gamma \tilde{G}
 \end{aligned}$$

is dominant process. There are three unknown masses ($m(\tilde{\chi}_2^0)$, $m(\tilde{\ell}_R)$ and $m(\tilde{\chi}_1^0)$) in this chain. Figures 14 show the invariant mass distributions of $\ell\ell$, $\ell\gamma$ and $\ell\ell\gamma$. Two kinematic edges and two end points, $M_{\ell\ell}^{max}$, $M_{\ell\gamma}^{(1)max}$, $M_{\ell\gamma}^{(2)max}$, and $M_{\ell\ell\gamma}^{max}$ are clearly observed in these three distributions. These edges and end points are related to three unknown masses.

$$\begin{aligned}
 M_{\ell\ell}^{max} &= m(\tilde{\chi}_2^0) \sqrt{1 - (m(\tilde{\ell})/m(\tilde{\chi}_2^0))^2} \sqrt{1 - (m(\tilde{\chi}_1^0)/m(\tilde{\ell}))^2} \\
 M_{\ell\gamma}^{(1)max} &= m(\tilde{\ell}) \sqrt{1 - (m(\tilde{\chi}_1^0)/m(\tilde{\ell}))^2} \\
 M_{\ell\gamma}^{(2)max} &= m(\tilde{\chi}_2^0) \sqrt{1 - (m(\tilde{\ell})/m(\tilde{\chi}_2^0))^2} \\
 M_{\ell\ell\gamma}^{max} &= \sqrt{m(\tilde{\chi}_2^0)^2 - m(\tilde{\chi}_1^0)^2}
 \end{aligned} \tag{6}$$

All three masses can be determined very precisely (0.1%) by fitting four end points(1C fit).

There are three unknown momentum components in each \tilde{G} , but these are also three constraints ($m(\tilde{\chi}_2^0)$, $m(\tilde{\ell}_R)$ and $m(\tilde{\chi}_1^0)$). Thus, \tilde{G} momentum can be solved event by event. Solution has 4-fold ambiguity due to a quadratic equations and choice of lepton. This ambiguity can be solved [14]

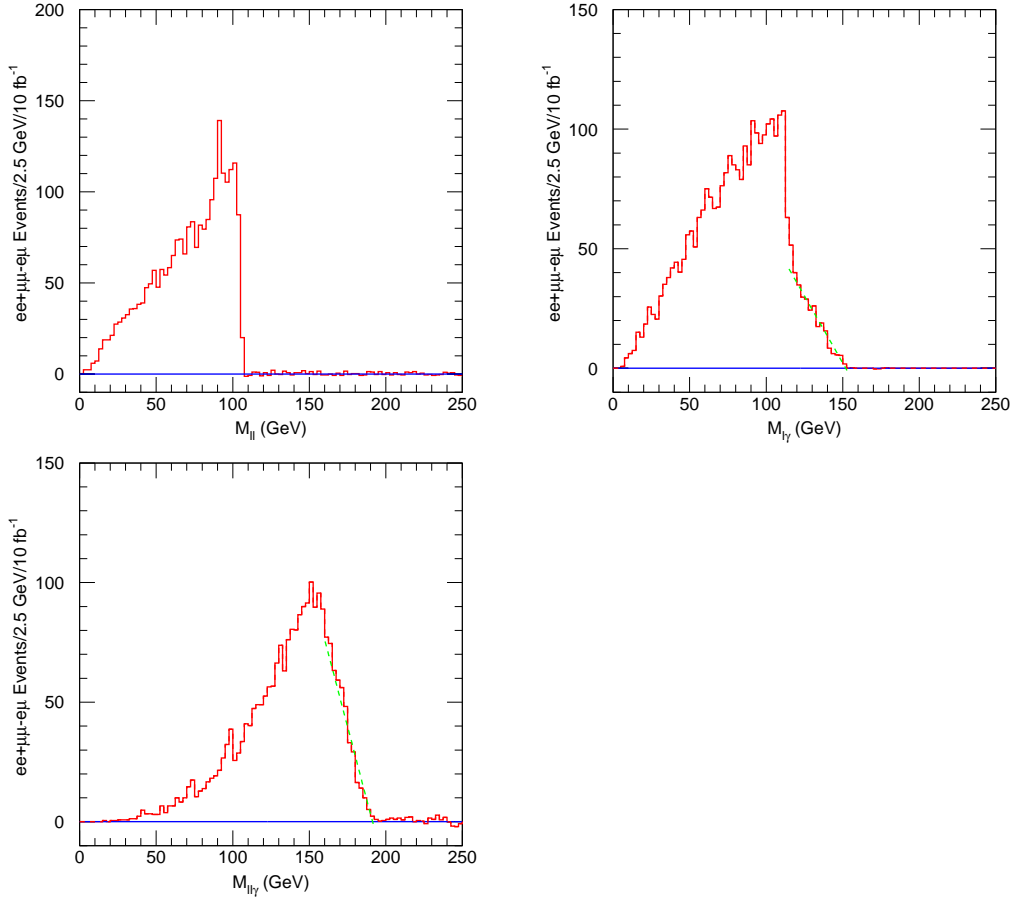


Figure 14: Invariant mass distributions of ll , $l\gamma$ and $ll\gamma$ ($\sqrt{F}=210 \text{ TeV}$, $M_m=500 \text{ TeV}$, $N_5=1$ and $\tan\beta=5$)

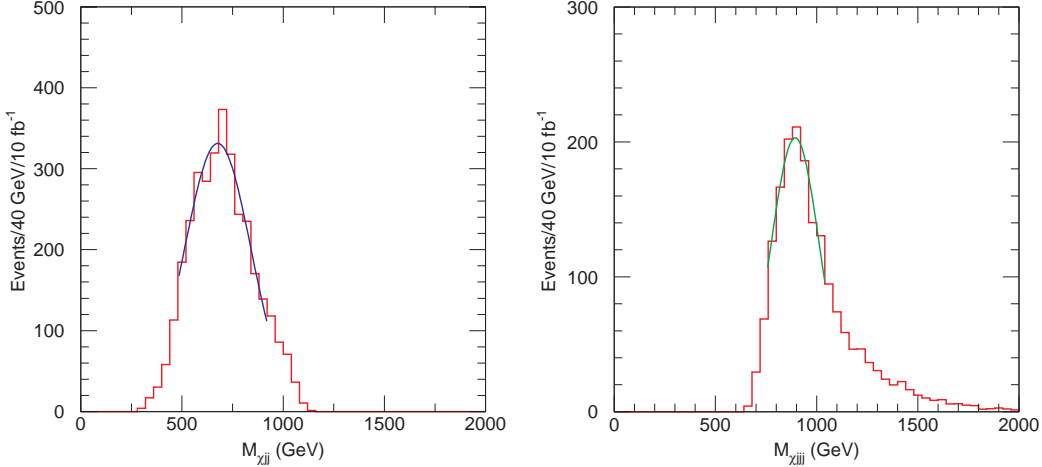


Figure 15: Invariant mass distributions of $jj\tilde{\chi}_2^0$ and $jjj\tilde{\chi}_2^0$

using \cancel{E}_T measurement, and events are fully reconstructed event by event. $\tilde{\chi}_2^0$ is emitted from $\tilde{q} \rightarrow q\tilde{g}(\rightarrow q\tilde{q}\tilde{\chi}_2^0)$ decay chain. Figures 15 show the invariant mass distributions of $jj\tilde{\chi}_2^0$ and $jjj\tilde{\chi}_2^0$. Peaks appear at $m(\tilde{g})$ and $m(\tilde{q})$ as shown in the figures, and these can be determined directly.

The Lifetime of NLSP has an information about SUSY breaking scale, and it is a critical parameter in the GMSB models. When $\tilde{\chi}_1^0$ has a short lifetime of $c\tau \sim 1\text{mm}$, the Dalitz decay of $\tilde{\chi}_1^0 \rightarrow \tilde{G}e^+e^-$ can be used to find out the decay point. The sensitivity is only limited by the resolution of the vertex detector, and measurement can be performed up to $O(100)\mu\text{m}$. A $\tilde{\chi}_1^0$ decaying inside the tracking volume produces non-pointing γ . The γ does not point to the primary vertex and detection timing in the EM calorimeter is also delayed. Deviation angle of pointing and delay time of the detection are shown in Fig. 16. Although $c\tau$ of $\tilde{\chi}_2^0$ is as long as 1.1km, long tails are observed in both distributions. These tails are significant compared to the resolutions ($\Delta\Theta = 60\text{mrad}/\sqrt{E(\text{GeV})}$ and $\Delta t = 0.1\text{ nsec}$). The Lifetime can be measured using these distributions, and we have sensitivity up to $c\tau \sim 100\text{ km}$.

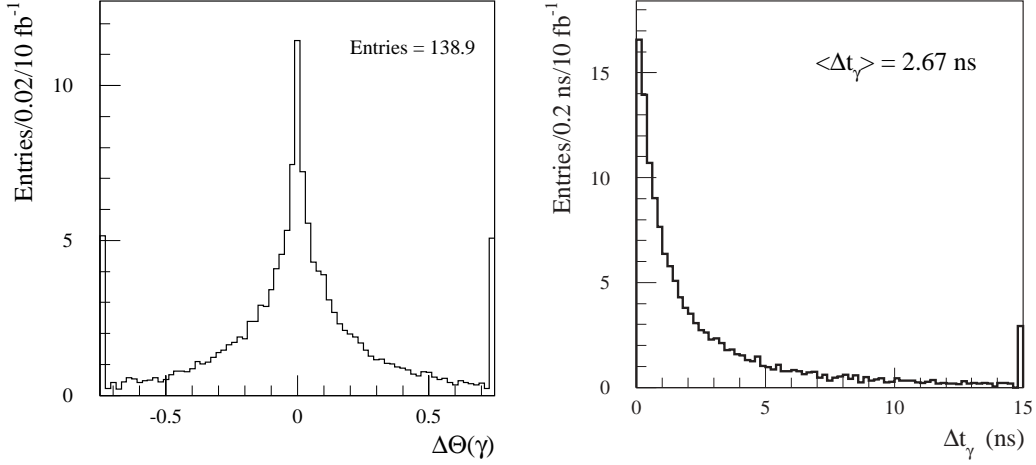


Figure 16: Deviation angle of pointing (left) and delay time of detection (right) for $\tilde{\chi}_1^0 \rightarrow \tilde{G}\gamma$ with $c\tau=1.1\text{km}$.

4.3 Heavy charged stable particle:

If NLSP is $\tilde{\ell}(\tilde{\tau}$ for large $\tan\beta$ case), whose lifetime is longer than $O(1)$ m, some part of $\tilde{\ell}$ decay outside detectors. Time-of-flight of heavy charged particles is longer than TOF of muon, and this delay time, ΔT , can be measured by hit-pattern in muon chambers. Time resolution of muon system is about 1 nsec. A velocity and mass can be determined by ΔT and momentum.

$$1/\beta = 1 + c\Delta T/d$$

$$M^2 = (1/\beta^2 - 1)p^2 \quad (7)$$

Scatter plot of $1/\beta$ vs momentum and distribution of the reconstructed mass are showed in Fig. 17 for $\tilde{\tau}$ signal with three different $m(\tilde{\tau})$'s. $\tilde{\tau}$ can be discovered from 90 to about 700 GeV [19] with $L=100\text{fb}^{-1}$. A Lifetime of $\tilde{\tau}$ can be measured by counting the number of events with one and two observed stable $\tilde{\tau}$'s.

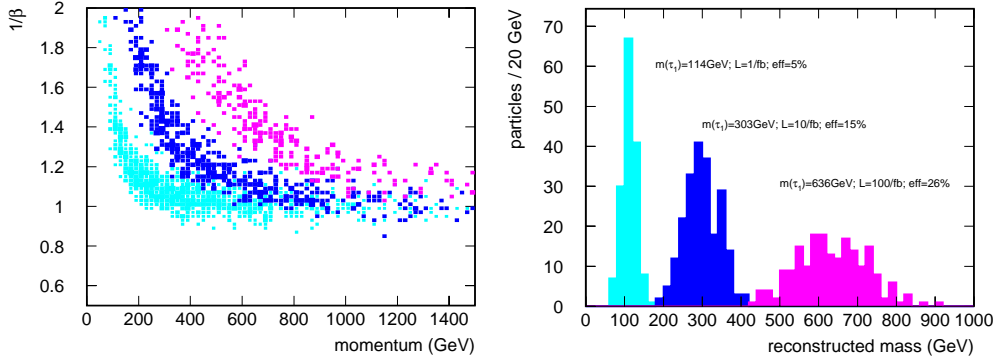


Figure 17: (Left) scatter plot of $1/\beta$ vs momentum (Right) reconstructed mass distributions for long lifetime $\tilde{\tau}$ ($m=114,303$ and 636 GeV)

5 R-parity Violation

In the previous three models, R-parity [7] is assumed to be conserved. Then LSP is stable and \cancel{E}_T is essential experimental signature. But if R-parity is not conserved, LSP can decay inside detector, and \cancel{E}_T can not be used for the SUSY hunting. Following three couplings violate R-parity and baryon/lepton numbers,

- $\lambda_{ijk} L^i L^j E^k: \tilde{\chi}_1^0 \rightarrow \ell^+ \ell^- \nu$
- $\lambda'_{ijk} L^i Q^j D^k: \tilde{\chi}_1^0 \rightarrow \ell(\nu) q \bar{q}$
- $\lambda''_{ijk} U^i D^j D^k: \tilde{\chi}_1^0 \rightarrow q \bar{q} q$

where L(Q) and E(D) are respectively isodouble and isosinglet lepton(quark), and index (i,j,k) means the generation.

If $\lambda''_{ijk} \neq 0$, $\tilde{\chi}_1^0$ decays into three jets and no \cancel{E}_T is expected (difficult case at LHC). It is possible, however, to extract SUSY signals using the following cascade decay involving leptons;

$$\begin{aligned} \tilde{q}_L &\rightarrow \tilde{\chi}_2^0 q \\ &\rightarrow \tilde{\ell} \ell \end{aligned}$$

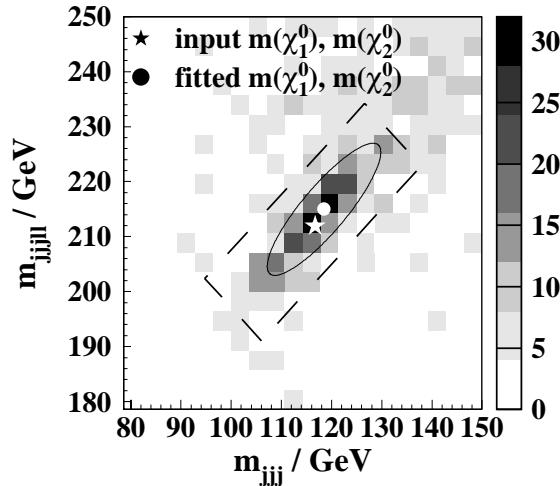


Figure 18: 2D-plot of M_{jjj} and $M_{jjj\ell^+\ell^-}$.

$$\begin{aligned} &\rightarrow \tilde{\chi}_1^0 \ell \\ &\rightarrow q\bar{q}q . \end{aligned}$$

Large excess is expected beyond the standard model processes in the $\sum_{jets} p_T + \sum_{lepton} p_T$ distribution, after requiring multiple jets ($N_{jets} = 8 \sim 10$) plus multiple leptons ($N_\ell > 2$). It is also possible to reconstruct $\tilde{\chi}_1^0 \rightarrow q\bar{q}q$ and $\tilde{\chi}_2^0 \rightarrow \ell^+\ell^-\tilde{\chi}_1^0$ processes [20]. Figure 18 shows 2D-plot of M_{jjj} and $M_{jjj\ell^+\ell^-}$, and a peak can be observed at $m(\tilde{\chi}_1^0)$ and $m(\tilde{\chi}_2^0)$. LHC has a good potential even if R-parity is violated.

6 Conclusions

Supersymmetry should be discovered at LHC, if \tilde{g} and \tilde{q} are lighter than about 2 TeV. Signals will be, perhaps, found not only in the $(\cancel{E}_T + jets)$ channel but also in $(\cancel{E}_T + jets + lepton(s))$ channels.

Exclusive studies have been performed in mSUGRA and GMSB models. $\tilde{\chi}_2^0$ plays important role to determine masses of the SUSY particles, and studies has been done systematically. In many cases, it should be possible to measure many combinations of masses of SUSY particles from various

kinematic distributions. Masses of \tilde{g} , \tilde{q} , $\tilde{\ell}$, $\tilde{\chi}_2^0$ and $\tilde{\chi}_1^0$ can be determined with help of model. Accuracies of these masses are about a few–10%. When there are at least three 2-body decay, masses can be determined model-independently. Lifetime of NLSP also can be measured in the GMSB model, giving an information of the SUSY breaking scale.

Event topologies involving 3rd generation are complicated, but these will provide good knowledges about Higgsino and trilinear coupling. Furthermore, measurements of decay branching fractions will give redundant informations of SUSY parameters, and redundancy is very important to examine the SUSY models. Systematic studies on both subjects are necessary.

References

- [1] General Reviews: H.P. Nilles, Phys. Rep. **110** (1984) 1
H.E. Haber and G.L. Kane, Phys. Rep. **117** (1985) 75.
- [2] ATLAS Technical proposal, CERN/LHCC/94-43.
- [3] CMS Technical proposal, CERN/LHCC/94-38.
- [4] S. Abel et al., hep-ph/0003154 for review
L. Alvarez-Gaume, J. Polchinski and M.B. Wise, Nucl. Phys. **B221** (1983) 495
L. Ibanez, Phys. Lett. **B118** (1982) 73
J. Ellis, D.V. Nanopolous and K.Tamvakis, Phys. Lett. **B121** (1983) 123.
- [5] General Reviews: G. Jungman, M. kamionkowski and K. Griest, Phys. Rept. **267** (1996) 195.
- [6] M. Dine, W. Fischler and M. Srednicki, Nucl. Phys. **B189** (1981) 575
S. Dimopoulos and S. Raby, Nucl. Phys. **B192** (1981) 353
C. Nappi and B. Ovrut, Phys. Lett. **B113** 175
L. Alvarez-Gaume, M. Claudson and M.B. Wise, Nucl. Phys. **B207**

- (1982) 961
M. Dine and A.E. Nelson, Phys. Rev. **D48** (1993) 1227
M. Dine, A.E. Nelson and Y. Shirman, Phys. Rev. **D51** (1995) 1362
M. Dine et al., Phys. Rev. **D53** (1996) 2658
- [7] P. Fayet, Phys. Lett. **B69** (1977) 489.
- [8] M. Drees and K. Hikasa, Phys. Lett. **B252** (1990) 127
K. Hikasa and M. Kobayashi, Phys. Rev. **D36** (1987) 724
A. Bartl, W. Majerotto and W. Porod, Z. Phys. **C64** (1994) 499.
- [9] E. Eichten et al., Rev. Mod. Phys. **56** (1984) 579.
- [10] M. Spira, Nucl. Phys. Proc. Suppl. **89** (2000) 222.
- [11] H. Baer, F.E. Paige, S.D. Protopopescu and X. Tata, hep-ph/0001086 (2000).
- [12] S. Mrenna, Comp. Phys. Comm. **101** (1997) 232
T. Sjöstrand, Comp. Phys. Comm. **82** (1994) 74.
- [13] D.R. Tovey, Phys. Lett. **B498** (2001) 1.
- [14] ATLAS Physics TDR, CERN/LHCC/99-15.
- [15] S. Abdullin et al., CMS/Note/98-006, hep-ph/9806366.
- [16] M. Nojiri, D. Toya, and T. Kobayashi, Phys. Rev. **D62** (2000) 075009.
- [17] By A. Djouadi, Y. Mambrini and M. Muhlleitner Eur. Phys. J. **C20** (2001) 563.
- [18] B.C. Allanach, C.G. Lester, M.A. Parker and B.R. Webber CERN-TH-2000-149 (2000).
- [19] M. Kazana, G. Wrochna and P. Zalewski, CMS/CR/1999-019.
- [20] B.C. Allanach et al. JHEP **0103** (2001) 048.